'Period doubling' induced by optimal control in a behavioral SIR epidemic model

Sileshi Sintayehu Sharbayta [a,*], Bruno Buonomo [b], Alberto d'Onofrio [c,d,*], Tadesse Abdi [a]

[a] Department of Mathematics, Addis Ababa University, Addis Ababa, Ethiopia
[b] Department of Mathematics and Applications, University of Naples Federico II, via Cintia, I-80126 Naples, Italy
[c] Department of Mathematics and Geosciences, University of Trieste, via A. Valerio, 12, I-34127 Trieste, Italy
[d] Department of Mathematics and Statistics, Strathclyde University, Glasgow, Scotland, UK

ARTICLE INFO

Article history:
Accepted 13 June 2022

Keywords:
Period doubling
Sub-harmonic resonance
Optimal control
Social distancing
Behavior

ABSTRACT

We consider a behavioral SIR epidemic model to describe the action of the public health system aimed at enhancing the social distancing during an epidemic outbreak. An optimal control problem is proposed where the control acts in a specific way on the contact rate. We show that the optimal control of social distancing is able to generate a period doubling–like phenomenon. Namely, the 'period' of the prevalence is the double of the 'period' of the control, and an alternation of small and large peaks of disease prevalence can be observed.

1. Introduction

In the last fifty years, the field of Mathematical Epidemiology (ME) has become increasingly important as a decision supporting tool for public health authorities [1–4]. However, in the last twenty years it gradually increased the awareness that even the most sophisticated models needed a further layer to correctly represent reality: the inclusion of human behavior. Indeed, in classical epidemic models the contagion is modeled as a chemical reaction and the vaccination is represented as constant rate or as a given function of time. These assumptions are not adequate to represent modern scenarios where private choices are the outcome of conflicting instances. Therefore, in the last few years a new branch of ME, termed the *behavioral epidemiology of infectious diseases* (BEID), was born [4,5]. The first pioneering model in ME which included explicitly the human behavior was the one proposed by Capasso and Serio [6]. In their well known work it is assumed that the epidemic outbreak may be affected by social distancing. This phenomena was described through a *force of infection* (i.e. the per capita rate at which susceptibles contract the infection) given by a nonlinear function of the current prevalence of the disease.

In the paper [7], the Capasso and Serio's model was extended in two directions. First, the authors considered an endemic disease scenario, which is typical of childhood diseases; second, they modeled the contact rate as a function of the available information not only on the present but also on the past disease prevalence. Indeed, the decision to adopt the social distancing measure is taken by the agents on the basis of their overall '*memory*' of the disease spread (as typically happens for vaccine–related decisions). Therefore, the extended model includes an additional state variable: the so called *information index M*, which was previously introduced in [8] in the context of a behavioral model of childhood vaccination. Of course, in the context of behavioral models based on the index *M*, the way in which the memory is modeled is a key aspect, as the dynamics of the system depends critically on that. The main result presented in [7] is that social behavior changes alone can trigger sustained oscillations.

It is worth pointing out that quite naturally BEID has become a prominent tool of modeling COVID-19 pandemics starting from the work [9].

Another important and very active area of ME is the application of the Optimal Control (OC) theory [10–13]. This area combines analytical mechanics, infectious disease modeling, decisions sciences and health economics. The application of OC to epidemiological problems is especially useful when planning public health interventions aimed at reducing both the health and the economic impacts of the target diseases. The OC theory is nowadays a classical tool in ME of infectious diseases [10,

* Corresponding authors.
E-mail addresses: sileshi.sintayehu@aau.edu.et (S.S. Sharbayta), alberto.donofrio@units.it, alberto.d-onofrio@strath.ac.uk (A. d'Onofrio).

14–27]. It has been proposed also in Economics [28,29] where the costs are modeled in a way similar to that outlined above. Among the most promising recent areas of application of OC to ME we mention the OC of fractional epidemic systems [30,31] and the design of OC-based strategies in the management of current COVID-19 pandemic [32–34].

The OC theory can be fruitfully applied even in the context of BEID, although this area of applications is still in its infancy. In this direction, some pioneering investigations aimed at favoring vaccine uptake can be found in the literature [35–37], as well as some papers focused on the optimal shape of social distancing [33,38–41].

We conclude this overview by mentioning a third key area of ME: the study of the impact of seasonality on the dynamics and control of the disease. As a matter of fact, one of the most important and best known result of ME is that the rich variety of oscillatory phenomena found in many important epidemiological time series can arise not just by chance but from simple deterministic phenomena as the seasonality of weather and the school calendar [42–46]. These phenomena can simply be modeled as periodic fluctuations of the contact rate. As a consequence, such complex dynamics can be explained by classical analytical mechanics: a nonlinear dynamical system periodically forced with a period T can exhibit solutions with periods that are integer multiples of T [47–52]. Such phenomenon is called sub-harmonic resonance (see the outstanding pioneering works [53–56]), and sometime can bifurcate in chaotic solutions via period–doubling bifurcation [48,49,52]. In particular, in ME the alternation of years of large epidemic outbreaks with years characterized by small epidemic outbreaks can be explained as a sub-harmonic resonance due to seasonally fluctuating contact rates [44,46, 57,58].

In this work, we propose a theoretical OC problem of social distancing based on a BEID model and show that a period doubling–like phenomenon may occur. Namely, giving a finite time horizon, the OC obtained by imposing the Pontryagin's conditions tends to a '*periodic*' behavior that, in turn, induces a '*period doubling*' phenomenon where the alternation of small and large outbreaks of the disease prevalence (and of the information index) can be observed. We used the quotation marks since a genuine period doubling would require an infinite interval, of course.

At the best of our knowledge, this is the first time that such a phenomenon has been reported in the literature.

The paper is organized as follows: in Section 2 we summarize the content of paper [7], i. e. we recall the basic uncontrolled BEID model and its basic properties; in Section 3 we introduce the controlled model; in Section 4 we analyze the impact of a simple constant control; in Section 5 the OC problem is introduced; in Section 6 we show some preliminary short–term numerical simulations; in Section 7 the phenomenon of OC–induced doubling sub-harmonic resonance is illustrated. Finally, concluding remarks ends this contribution.

2. Background: the model by d'Onofrio and Manfredi (2009)

In this Section we briefly recall the properties of the behavioral SIR epidemic model proposed by d'Onofrio and Manfredi [7]. The total population is assumed to be constant (birth rate is equal to death rate) so that the model reads:

$$\dot{S} = \mu(1 - S) - \beta(M)IS \tag{1}$$

$$\dot{I} = \beta(M)IS - (\mu + \nu)I \tag{2}$$

$$R = 1 - S - I, \tag{3}$$

where $S(t)$, $I(t)$ and $R(t)$ denote the fractions of susceptibles, infectious and removed individuals at time t, respectively; μ and ν are positive constants representing the birth/death rate and the recovery rate, respectively. The function $\beta(M)$ is the transmission rate, which includes the contact rate (and therefore is influenced by social distancing) and depends on the information index $M(t)$. This index describes the information regarding the status of the disease in the community and is a function of the present and past values of the state variables. It is given by:

$$M(t) = \int_0^{+\infty} F(S(t-\tau), I(t-\tau))K(\tau)d\tau, \tag{4}$$

where $K(x)$ is a memory kernel that weight the past values. In particular, in [7] the authors investigated the case where

$$F(S, I) = I, \tag{5}$$

and three different memory kernels, the *Dirac kernel*, the *weak Erlang kernel* and the *strong Erlang kernel*.

i) *Dirac kernel*, $K(t) = \delta(t)$. This kernel implies that $M = I$, so that the transmission rate is assumed to depend only on the current information on the disease spread. This means that the individuals' decision to adopt the social distancing measure is based only on the knowledge of the current information on the disease spread. In this case model (1)-(2)-(4) becomes an extension of the epidemic model proposed by Capasso and Serio [6]; *ii*) the *weak Erlang kernel*, $K(t) = ae^{-at}$. In this case the weight of past information is exponentially fading; *iii*) the *strong Erlang kernel* (or Erlang kernel of order two),

$$K(t) = a^2 te^{-at}. \tag{6}$$

An interpretation of this kernel is that the current information is unavailable and that the maximum weight is assigned at the information arrived to the public after a characteristic time $T = 2/a$.

In [7] it was shown that, regardless of the specific kernel adopted, the disease–free equilibrium (DFE) $E_0 = (1, 0)$ of model (1)–(2) is globally stable provided that $\beta(0) < \mu + \nu$. On the contrary, if $\beta(0) > \mu + \nu$, then the DFE is unstable and the model admits a unique endemic equilibrium.

The numerical simulations provided in [7] are performed in the particular case where the contact rate is given by:

$$\beta(M) = \frac{\beta_0}{1 + \alpha\frac{M}{I_{SIR}}}, \tag{7}$$

where the parameter β_0 is the contact rate of the basic SIR model (therefore it represents the baseline contact rate in absence of information about the disease spread) and I_{SIR} denotes the endemic prevalence of the basic SIR model with contact rate β_0, that is:

$$I_{SIR} = \frac{\mu}{(\mu + \nu)}\left[1 - \frac{\mu + \nu}{\beta_0}\right].$$

3. The model with control

We assume that the public health system (PHS) can enact actions aimed at reducing the contact rate and that a control function $u(t)$ summarizes such actions. Taking into account that the transmission rate can be seen as the product of the contact rate and the probability that a contact with a susceptible individual results in transmission, it follows that it can be described by a strictly decreasing function of u, say $\beta(M, u)$.

There are at least two possible ways to represent this function. The first way is to assume that the contact rate depends only on the control, say $\beta(u)$ (e.g. it linearly decreases as the control $u(t)$ increases). This approach has been explored by some authors [33,59]. The second way is to assume that the PHS actions increase the sensitivity of citizens with

respect to the news on the disease spread. This means that the parameter α in (7) must be modulated. We choose this second approach, which is not explored at all in the literature. Namely, we can rewrite the expression (7) as follows:

$$\beta(M) = \beta_0 \frac{M_{50}}{M_{50} + M},$$

where $M_{50} = I_{SIR}/\alpha$ is the information value that halves the baseline contact rate (i.e. $\beta(M_{50}) = \beta_0/2$). As mentioned above, it is reasonable to think that the public health system enacts actions represented by a control function (say – for the moment – $\widehat{u}$) aimed at increasing the sensitivity of the population to the information, i.e. the effect of such actions is to decrease the value of M_{50}. Therefore we get:

$$\beta(M, \widehat{u}) = \beta_0 \frac{M_{50}(\widehat{u})}{M_{50}(\widehat{u}) + M}.$$

From this we get:

$$\beta(M, \widehat{u}) = \beta_0 \frac{1}{1 + \widehat{\alpha}(\widehat{u}) M}.$$

Finally we study the model under the simplest case where $\widehat{\alpha}(\widehat{u})$ is a linear function of the control $\widehat{u}$, i.e.

$$\widehat{\alpha}(\widehat{u}) = \frac{\alpha}{I_{SIR}}(1 + b\widehat{u}).$$

In the following, for the sake of simplicity, we take the control as the quantity

$$u = b\widehat{u}.$$

This leads to the following form modification of the contact rate (7):

$$\beta(M, u) = \frac{\beta_0}{1 + \alpha(u+1)\frac{M}{I_{SIR}}}, \tag{8}$$

where the positive parameter α tunes the degree of change of contact patterns.

Using (5), model (1)-(2)-(4) becomes:

$$\dot{S} = \mu(1 - S) - \beta(M, u) I S \tag{9}$$

$$\dot{I} = \beta(M, u) I S - (\mu + \nu) I \tag{10}$$

$$M = \int_0^{+\infty} I(t - \tau) K(\tau) d\tau, \tag{11}$$

where $\beta(M,u)$ is given by (8).

Here, we will focus on the case of strong Erlang kernel, although when appropriate we will give some information on the dynamics of model (9)-(10)-(11) under both the Dirac and weak Erlang kernels.

4. The case of constant control

In this section we consider the case of constant control in order to explore some general features of the model. We begin by observing that when $u(t) = u$ (const.) the model has a unique endemic equilibrium regardless of the delay kernel adopted, as it can be easily checked by adapting the results obtained for $u = 0$ in [7]. The endemic equilibrium is:

$$E_e(u) = (S_e(u), I_e(u), M_e(u)) = \left(\frac{\mu + \nu}{\beta(I_e(u), u)}, I_e(u), I_e(u) \right), \tag{12}$$

where

$$I_e(u) = \frac{\mu(R_0 - 1)}{\frac{\mu\alpha(u+1)}{I_{SIR}} + \beta_0}, \tag{13}$$

and

$$R_0 = \frac{\beta_0}{\mu + \nu}, \tag{14}$$

is the basic reproduction number of the uncontrolled model (i.e. when $u = 0$).

As for the stability of E_e, since the effect of the constant control is simply to 'amplify' the value of the parameter α, we can use the analytical and numerical results contained in [7,60] and state that:

(i) in case of Dirac kernel, the endemic equilibrium is globally asymptotically stable (GAS) [7];
(ii) in case of weak Erlang kernel, the endemic equilibrium is locally asymptotically stable (LAS) [7]. Such an equilibrium is also GAS if some specific conditions on the parameters, as reported in [60], are satisfied;
(iii) in case of strong Erlang kernel, for $R_0 > 1$ the system is strongly persistent. Moreover, for any given value of u, the stability of the endemic equilibrium depends on the Erlang parameter a as described in [7], i. e. Hopf bifurcations can occur and the model may exhibit Yakubovich oscillations [61,62].

The strong Erlang kernel is the most interesting case. In Fig. 1 (left panel), a numerical simulation shows the region of stability and instability of the equilibrium $E_e(u)$ in the (u,α) plane, for a given set of parameter values and $a = 1/30$. In Fig. 1 (right panel) the same is shown for $\alpha = 0.4$. Note that at the boundary of the LAS regions a Hopf bifurcation occurs.

In Fig. 2 (where $a = 1/30$ and $\alpha = 0.4$), it can be seen the time courses of the state variables for: *i*) $u = 1.220$ (left panel), which is a value slightly below the instability threshold $u_* = 1.252$; *ii*) $u = 1.3$ (central panels), which is slightly over the instability threshold; *iii*) $u = 10$ (right panel). The limit cycle of the simulated time–series for $t \in (58000, 60000)$ corresponding to $u = 1.3$ and $u = 10$ are depicted in Fig. 3, left and right panel, respectively.

5. Optimal control of the disease spread

We now investigate the time profile of the control $u(t)$ as result of an OC problem. Only the (more interesting) case of strong Erlang kernel will be considered. In this case, by applying the so-called *linear chain trick* [63], the model (9)-(10)-(11) becomes the following system:

$$\begin{aligned} \dot{S} &= \mu(1 - S) - \beta(M, u) I S \\ \dot{I} &= \beta(M, u) I S - (\mu + \nu) I \\ \dot{M}_1 &= a(I - M_1) \\ \dot{M} &= a(M_1 - M). \end{aligned} \tag{15}$$

The preliminary key problem of OC is the definition of the cost functional to be minimized. We assume, for the sake of simplicity, that only the following two costs are included in the functional:

i) *the cost associated to susceptibles that becomes infectious*, which is represented by:

$$J_1(u) = \int_0^T K_I N \beta(M(t), u(t)) S(t) I(t) dt, \tag{16}$$

where T is the time horizon, K_I is the cost payed by PHS for a single infection and N denotes the total population;

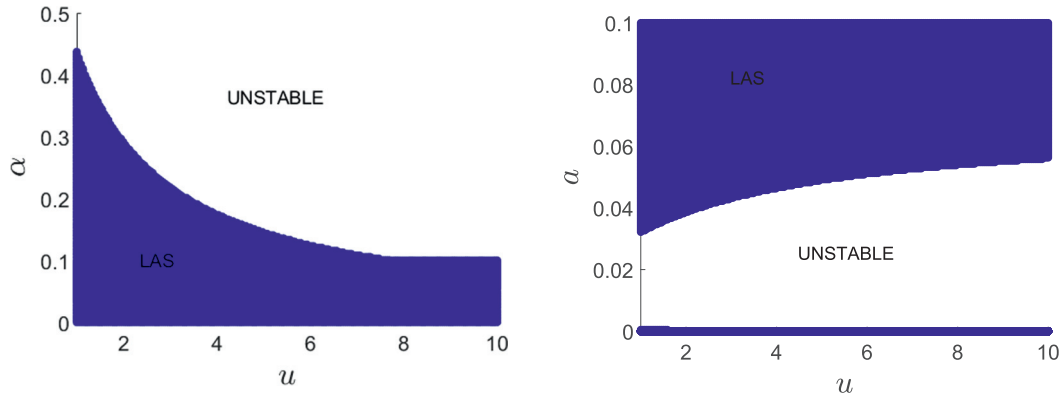

Fig. 1. Impact of the constant control u on the stability of the endemic equilibrium $E_e(u)$ given in (12). White area indicates the instability region; blue area indicates the stability region. Left panel: dependence of the LAS on the parametric pair (u,α) for $a = 1/30$; right panel: dependence of the LAS on the parametric pair (u,a) for $\alpha = 0.4$. Other values of the parameters are as in Table 1.

ii) *the cost associated to the control*. We assume that it is of linear–quadratic type:

$$J_2(u) = \int_0^T \left(K_1 u(t) + K_2 u(t)^2\right) dt, \tag{17}$$

where K_1 and K_2 are parameters tuning the linear and quadratic intervention costs, respectively.

The assumption of a linear-quadratic cost is not extremely realistic but widespread used in the literature. Such an assumption is made, in particular, when a precise functional form for this cost is not known, as in our case. Nevertheless, in Section 7, we will include a numerical simulation where the cost is approximately linear (see Fig. 7, right panel).

Setting $K = K_I N$, the OC problem can be stated as follows: *find the control $u^*(t)$ such that it minimizes the functional under the dynamical constraint (15) and the further constraint*:

$$J(u) = J_1(u) + J_2(u) = \int_0^T \left[K\beta(M(t), u(t))S(t)I(t) + K_1 u(t) + K_2 u(t)^2\right] dt, \tag{18}$$

$$u \in U, \tag{19}$$

Where U, the set of admissible controls, is given by:

$$U = \{u(t) : 0 \le u_{\min} \le u(t) \le u_{\max} \mid u \text{ is Lebesgue integrable}, t \in [0,T]\}.$$

According to Pontryagin's local minimum principle [11,64,65], the function $u^*(t)$ that minimizes the cost functional (18) also minimizes the current value of the associated Hamiltonian, which is given by

$$\begin{aligned} H(x,u,\lambda) = \; & K\beta(M,u)SI + K_1 u + K_2 u^2 + \lambda_1[\mu(1-S) - \beta(M,u)IS] \\ & + \lambda_2[\beta(M,u)IS - (\mu+\nu)I] + \lambda_3 a(I - M_1) + \lambda_4 a(M_1 - M), \end{aligned} \tag{20}$$

where $x = (S,I,M_1,M)$, and $\lambda = (\lambda_1,\lambda_2,\lambda_3,\lambda_4)$ is the vector of the adjoint state variables. The latter solve the so called adjoint system

$$\dot{\lambda}_1 = \frac{\partial H}{\partial S}, \quad \dot{\lambda}_2 = \frac{\partial H}{\partial I}, \quad \dot{\lambda}_3 = \frac{\partial H}{\partial M_1}, \quad \dot{\lambda}_4 = \frac{\partial H}{\partial M}, \tag{21}$$

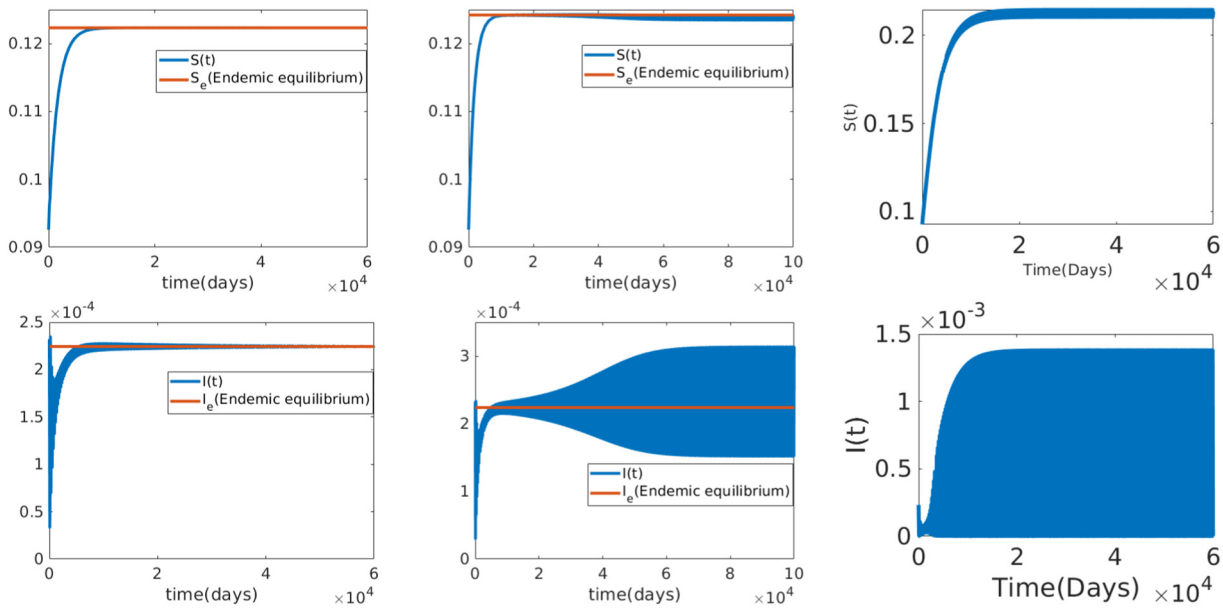

Fig. 2. Impact of the constant control u on the susceptibles S (upper panels) and on the infectious I (lower panels), for, $a = 1/30$, $\alpha = 0.4$. Three values of u are considered: $u = 1.22$ (left panels), $u = 1.30$ (central panels) and $u = 10$ (right panels). Other parameter values are as in Table 1.

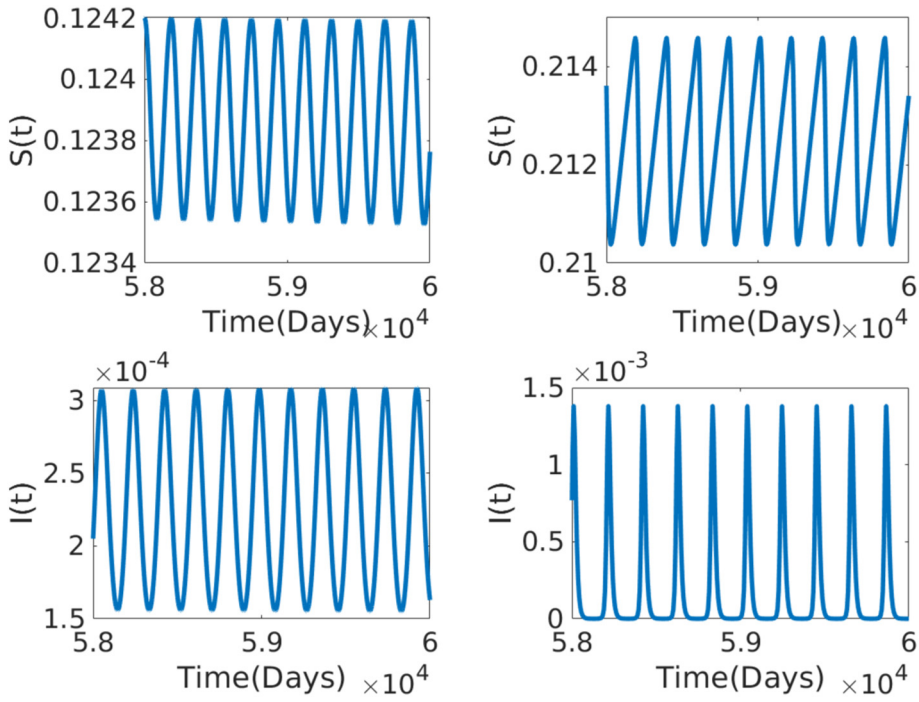

Fig. 3. The oscillatory dynamics of model (9)-(10)-(11) with constant control in the cases $u = 1.3$ (left panel) and $u = 10$ (right panel). These plots are the zoomed part of central and right panels of Fig. 2 for $t \in (58000,60000)$.

yielding:

$$\begin{aligned}
\dot{\lambda}_1 &= \lambda_1\mu + \beta(M,u)I(\lambda_1 - \lambda_2 - K)\\
\dot{\lambda}_2 &= \beta(M,u)S(\lambda_1 - \lambda_2 - K) + \lambda_2(\mu + \nu) - \lambda_3 a\\
\dot{\lambda}_3 &= a(\lambda_3 - \lambda_4)\\
\dot{\lambda}_4 &= h(M,u)IS(K - \lambda_1 + \lambda_2) + \lambda_4 a,
\end{aligned} \tag{22}$$

where

$$h(M,u) = \frac{\beta_0 I_{SIR}\alpha(u+1)}{(I_{SIR} + \alpha(u+1)M)^2}. \tag{23}$$

The transversality conditions reads:

$$\lambda_i(T) = 0, \quad i = 1,2,3,4. \tag{24}$$

The necessary condition for u^* to minimize the Hamiltonian is given by

$$\left.\frac{\partial H}{\partial u}\right|_{u^*} = 0, \tag{25}$$

where

$$\frac{\partial H}{\partial u} = \frac{\beta_0 I_{SIR}\alpha M}{(I_{SIR} + \alpha(u+1)M)^2} IS(\lambda_1 - \lambda_2 - K) + K_1 + 2K_2 u. \tag{26}$$

This quantity can be set in the form $\partial H/\partial u = P(u)/Q(u)$, so that condition (25) is satisfied if and only if u^* is such that

$$P(u) = Au^3 + Bu^2 + Cu + D = 0, \tag{27}$$

where

$$\begin{aligned}
A(S,I,M) &= 2K_2\alpha^2M^2,\\
B(S,I,M) &= 4K_2\left(\alpha^2M^2 + \alpha I_{SIR}M\right) + K_1\alpha^2M^2,\\
C(S,I,M) &= 2K_2(\alpha M + I_{SIR})^2 + 2K_1\left(\alpha^2M^2 + \alpha I_{SIR}M\right),\\
D(S,I,M) &= \beta_0\alpha I_{SIR}MIS(\lambda_1 - \lambda_2 - K) + K_1(\alpha M + I_{SIR})^2.
\end{aligned}$$

A positive solution, u^* of the Eq. (27) minimizes at least locally the Hamiltonian if and only if

$$\left.\frac{\partial^2 H}{\partial u^2}\right|_{u^*} > 0. \tag{28}$$

In our case we get:

$$\left.\frac{\partial^2 H}{\partial u^2}\right|_{u^*} = \frac{P'(u^*)}{Q(u^*)} - P(u^*)\frac{Q'(u^*)}{Q^2(u^*)} = \frac{P'(u^*)}{Q(u^*)} = \frac{3A(u^*)^2 + 2Bu^* + C}{Q(u^*)}.$$

Since $Q(u^*) > 0$, A, B and C are positive, and $3A(u^*)^2 + 2Bu^* + C > 0$ for all $u^* > 0$, it follows that if $u^* > 0$ is a solution of the Eq. (27), then it minimizes at least locally the Hamiltonian.

The Eq. (27) has only one positive real root if $D < 0$. That is:

$$K_1(\alpha M + I_{SIR})^2 < \beta_0\alpha I_{SIR}MIS(K + \lambda_2 - \lambda_1). \tag{29}$$

Therefore, for $D < 0$ the OC u^*, which is a solution of (27) and satisfies the given bounded interval ($u_{\min} \le u \le u_{\max}$), can be expressed as:

$$u^*(t) = \begin{cases} u_{\min}, & \text{if} \quad u^* \le u_{\min}\\ u^*, & \text{if} \quad u_{\min} < u^* < u_{\max}\\ u_{\max}, & \text{if} \quad u^* \ge u_{\max}. \end{cases} \tag{30}$$

For $D > 0$, the Eq. (27) has three or only one negative real roots, but no positive real roots. Therefore there are no positive real roots that can

Table 1
Parameters and their baseline values used for the numerical simulations.

Parameter	Description	Baseline value	Ref.
μ	Birth and death rate	1/75 year^{-1}	[7]
ν	Recovery rate	1/7 day^{-1}	[7]
R_0	Basic reproduction number	15	[7]
β_0	Baseline contact rate	$R_0(\mu+\nu)$	[7]
N	Total population	6×10^7	[36]
K_I	Average cost per infection	307 USD	[36]
K_1	Parameter tuning the linear intervention cost	750	Assumed
K_2	Parameter tuning the quadratic intervention cost	1500	Assumed
a	Delay parameter	1/30	[7]
$u_{\min}$	Minimum control	1	Assumed
$u_{\max}$	Maximum control	10	Assumed

minimize the Hamiltonian. Due to the restriction on the control ($u \geq u_{\min} \geq 0$) in this case the OC u^* can be taken as $u^* = u_{\min}$.

Remark 1. The second derivative of the Hamiltonian function (20) has not a globally defined sign, since the sign depends on the state and the adjoint state variables. As a consequence, we use a local form of the Pontryagin's principle. This means that the extremal u^* is a local minimum. However, this does not represent a major obstacle in achieving the results that we obtain in the next Section by means of numerical simulations.

6. Preliminary short–term numerical simulations

In Table 1 we list the baseline values of the parameters used in the numerical simulations. Some of them are taken from the literature while others (the bounds of the control, $u_{\min}$ and $u_{\max}$, and the tuning parameters, K_1 and K_2) are empirically determined, as follows.

First, we assume that the control u, which 'amplifies' the parameter α (see the expression of the transmission rate (8)), is at least able to double the value of α. Therefore we set $u_{\min} = 1$. We also empirically set $u_{\max} = 10$.

Second, we assess the impact of K_1 and K_2 on the cost functional in the case where the control u is constant and at time $t = 0$ the controlled system is at its steady state. In such a case formula (18) reads as follows:

$$J(u) = T\left[K\beta(M_e(u),u)S_e(u)I_e(u) + K_1u + K_2u^2\right], \tag{31}$$

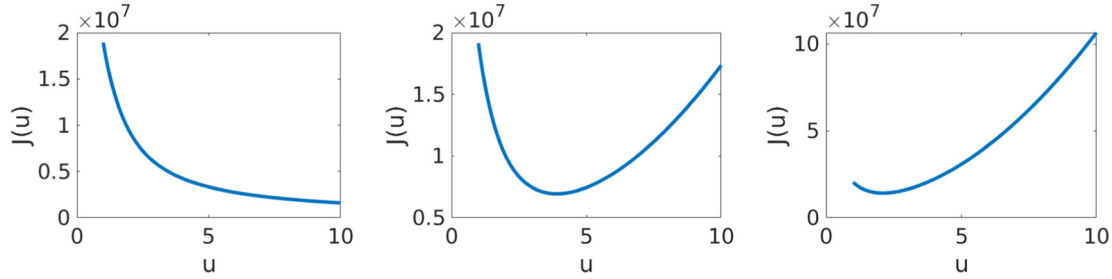

Fig. 4. Empirical choice of the pair (K_1,K_2) based on features of $J(u)$ under constant control and constraint $u \in (u_{\min},u_{\max})$. Left panel: $(K_1,K_2) = (0.5,1)$ (no proper minimum, but absolute minimum at $u = u_{\max}$); central panel: $(K_1,K_2) = (750,1500)$ (absolute minimum appropriately located close in–between $u = u_{\min}$ and $u = u_{\max}$); right panel: $(K_1,K_2) = (5000,1000)$ (absolute minimum close to $u = u_{\min}$). Here $T = 1$ and the other parameters are as in Table 1.

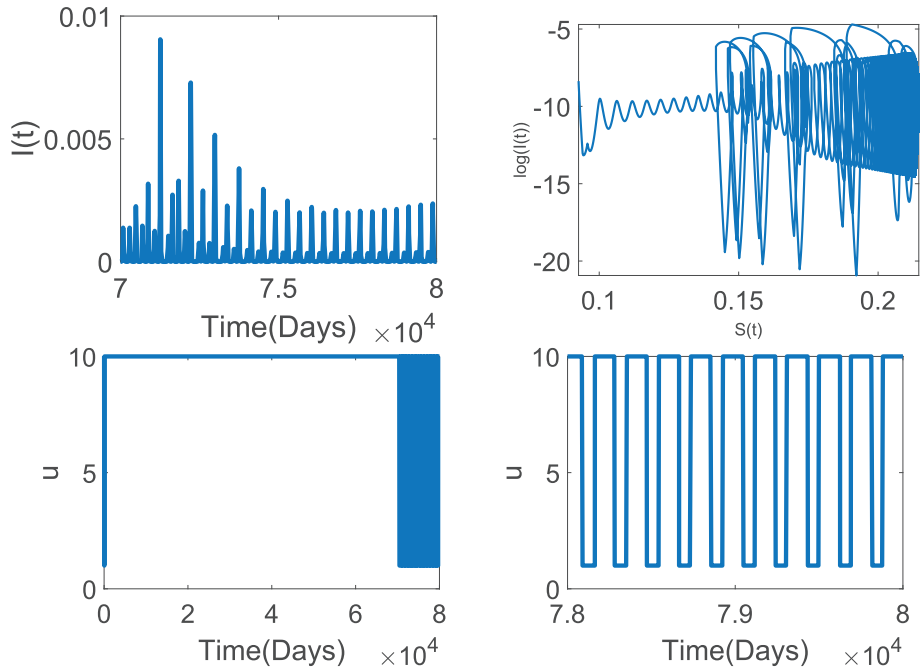

Fig. 5. Nonlinear resonance–like phenomenon induced by the OC. Scenario where the endemic equilibrium of the uncontrolled model is LAS. Left upper panel: prevalence $I(t)$; right upper panel: phase portrait $\log(I(t))$ vs $S(t)$; left lower panel: the OC $u_*(t)$; right lower panel: zoom of $u_*(t)$ for $t \in [78000,80000]$. Here $\alpha = 0.4$, $a = 1/30$ and the initial data are a close perturbation of $E_e(0)$ given in (12), i.e. $S(0) = 0.09259$, $I(0) = 2.32\times10^{-4}$, $M_1(0) = 2.32\times10^{-4}$, $M(0) = 2.32\times10^{-4}$. The other parameters are as in Table 1.

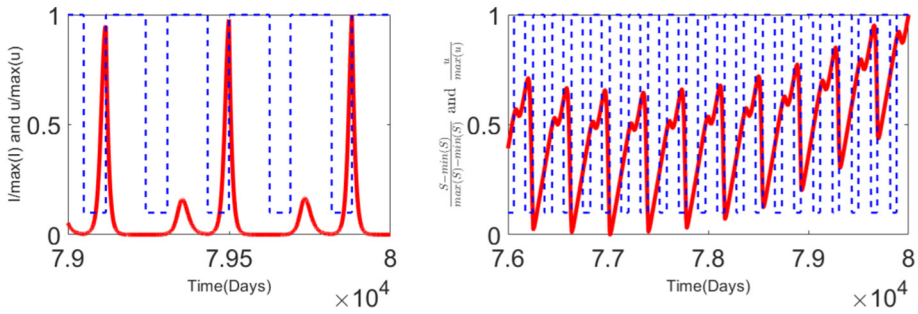

Fig. 6. 'Period doubling' behavior induced by OC. Scenario as in Fig. 5. Left panel: plot of $I(t)/\max(I)$ versus time (red line) and $u_*(t)/\max(u_*(t))$ versus time (blue line). Right panel: plot of $(S(t)-\min(S))/(\max(S)-\min(S))$ versus time (red line) and $u_*(t)/\max(u_*(t))$ versus time (blue line), where the symbols $\max(x)$ and $\min(x)$ denote the maximum and the minimum of the quantity x when t ranges in the interval indicated in the plots.

where the steady states of the state variables are given in (12). We empirically choose the values of the pair $(K_1,K_2)=(750,1500)$ such that under the constraint $u\in(u_{\min},u_{\max})$ the function $J(u)$ is such that a proper absolute minimum exists and it is not too close to $u_{\min}$ or to $u_{\max}$, as shown in Fig. 4.

Finally, in order to numerically solve the OC problem we employed the gradient descent (aka steepest descent) method [10] in conjunction with the fourth-order Runge-Kutta method (which we use to perform all the numerical integrations of the differential equations). Namely, we adapted the Matlab routines proposed in the book [10].

7. Period doubling

As shown in Fig. 5, the OC tends to be closer and closer to an approximately periodic square wave, whereas the corresponding value of prevalence tends to be closer and closer to an approximately periodic waveform with the alternation of large and small epidemic outbreaks. This suggest that the onset of a nonlinear resonances, and in particular subharmonic resonances, is induced by OC. Indeed, it is easy to verify that the pseudo–period of the recurrent 'periodic' prevalence is the double of the pseudo-period of the OC. Thus the specific form of nonlinear resonance observed is the well–known period doubling, often prodromic to chaos.

This can be clearly observed in Fig. 6 (left panel), which shows the normalized prevalence and the normalized OC. Interestingly, the large epidemic peak occurs in correspondence to the transition from $u_{\min}$ to $u_{\max}$ (which is not instantaneous but surely very rapid) that causes a drastic reduction of the prevalence. Later, when $u_*(t)$ switches back to $u_{\min}$, the prevalence begins to rise again and even though the control switch again to $u_{\max}$, a remarkable epidemic peak still occur. Finally, when $u_*(t)$ takes again the lower value $u_{\min}$, a very rapid growth of the prevalence is observed, which in turn is followed by a sudden increase of the control, and so on.

As for the dynamics of susceptibles $S(t)$, it presents an increasing pattern (due to the very slow demographic dynamics of $S(t)$) superimposed to a 'period doubling' pattern, see Fig. 6 (right panel). This 'period doubling' pattern is conserved across many parametric sets. For example, in Fig. 7 we compare the simulated time series of the information index $M(t)$ in the case where the cost functional is close to be purely quadratic ($(K_1,K_2)=(0.15,1500)$) with those obtained in the opposite scenario of a cost functional that is practically linear ($(K_1,K_2)=(750,0.01)$). The 'period doubling' is visible and becomes barely detectable only when $u_{\max}$ is small, as shown in Fig. 8.

Finally, Fig. 9 refers to a case where, in absence of control, model (15) oscillates. Notice that, as mentioned before, the time series of susceptible has an even more complex pattern of oscillations (see left panel of Fig. 9).

8. Concluding remarks

It is well–known that periodic forcing can induce various types of resonances in nonlinear dynamical systems, such as the sub-harmonic resonances [47–56], the most important of which is the period doubling [49,50]. The latter in turn is intimately related to the onset of chaos [52].

In mathematical epidemiology of infectious diseases, the period doubling effects are extremely important since outbreaks of pre–vaccine age childhood diseases sometime occurred with period two, where the alternation of small and large peaks is observed [42].

From a mathematical point of view, as first pointed out by London and Yorke [42] as well as by Smith, Schwartz and coworkers [43,44,46,57,58], this phenomenon can be explained as a period doubling response to a one–year special class of 'forcing': the spontaneous one–year fluctuations of the contact rate due to the school calendar.

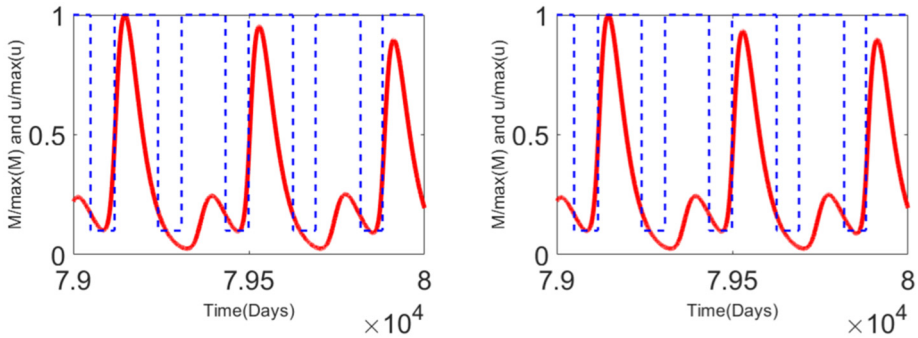

Fig. 7. Quadratic vs Linear cost functional: impact on the normalized time series of the information index $M(t)$. In both panels $M(t)/\max(M(t))$ versus time (red line) and $u_*(t)/\max(u_*(t))$ versus time (blue line), where the symbol $\max(x)$ denotes the maximum of the quantity x when t ranges in the interval indicated in the plots. Left panel: approximately quadratic cost functional ($(K_1,K_2)=(0.15,1500)$); right panel: approximately linear cost functional ($(K_1,K_2)=(750,0.01)$). The other parameters and initial conditions as in Fig. 5.

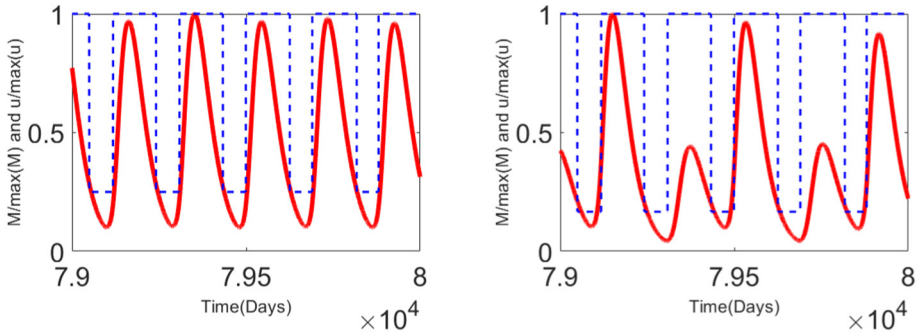

Fig. 8. Impact of the parameter $u_{\max}$ on the normalized time series of the information index $M(t)$. In both panels $M(t)/\max(M(t))$ vs time (red line) and $u_*(t)/\max(u_*(t))$ versus time (blue line), where the symbol $\max(x)$ denotes the maximum of the quantity x when t ranges in the interval indicated in the plots. Left panel: for $u_{\max} = 4$ the period doubling is barely detectable; right panel: for $u_{\max} = 6$ the period doubling is remarkable. The other parameters and initial conditions as in Fig. 5.

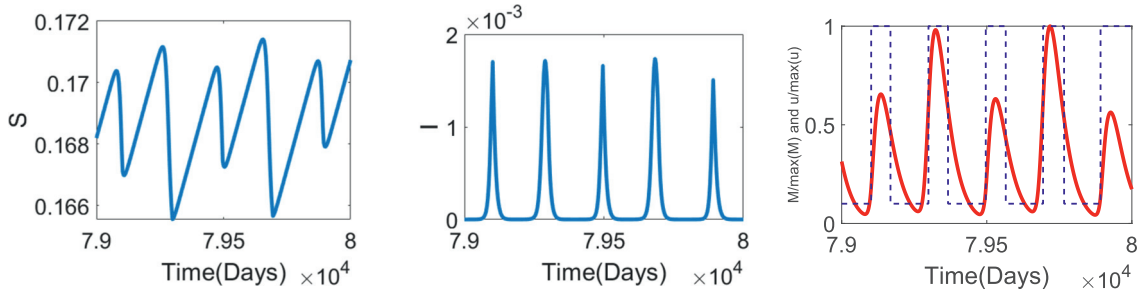

Fig. 9. Impact of the OC on a scenario where the uncontrolled model has a limit cycle ($\alpha = 1, a = 1/30$). Left panel: susceptibles $S(t)$; central panel: infectious $I(t)$; right panel: $M(t)/\max(M(t))$ versus time (red line) and $u_*(t)/\max(u_*(t))$ versus time (blue line), where the symbol $\max(x)$ denotes the maximum of the quantity x for t in the interval indicated in the plots. Other parameter values as in Table 1 and initial conditions: $S(0) = 0.1267$, $I(0) = 4.4352 \times 10^{-4}$, $M_1(0) = 2.9533 \times 10^{-4}$, $M(0) = 1.9941 \times 10^{-4}$.

In this paper, we obtain a particular period doubling of the disease prevalence as a response to the OC of social distancing in the context of a SIR endemic model. Therefore, the nature of forcing here is extremely different because the control u is the result of the OC procedure, which in turn is a function of the state variables of the OC–related Hamiltonian boundary values problem. In other words the 'periodicity' of the control u is not an a priori datum.

An interesting point is that the alternation of small and large epidemic peaks is easily interpretable since the periodic shape of the OC is practically a square–wave like. Of course, the notion of period doubling, which is usually rigorous, here is only approximate since the time horizon of the OC problem is not infinite. Note that our simulations suggest for the susceptibles $S(t)$ an even more complex pattern of oscillations (see Fig. 6, right panel), whereas the information index $M(t)$ also undergoes the above–mentioned 'period doubling' (see Fig. 8, right panel).

Our work has, of course, a number of limitations. In particular, we used a quite traditional description of costs, i.e. the cost functional is the sum of the costs associated to the PHS actions and the cost related to the number of infected subjects. This approach is different from the one currently used by some authors in health economy. These authors, indeed, although taking advantage of ME for the description of the spread of the infectious diseases, propose radically different cost functionals based on other and more modern indicators of costs [66–70]. Moreover, due to lack of data (especially regarding the costs of awareness campaigns) we have that: *i*) the assumption of linear-quadratic dependence of the control in the cost functional (18) is made only for the sake of plausibility and simplicity; *ii*) the numerical values of parameters in the cost functional are obtained on the basis of simple mathematical considerations. Therefore, from one hand this contribution is more a theoretical modeling work inspired by biology than a proper realistic model. On the other hand, the observed phenomena may be of some interest in the fields of Applied Dynamical systems, of ME and of applied OC theory.

CRediT authorship contribution statement

Term	SSS	BB	AD	TA
Conceptualization		✓	✓	
Methodology/Study design		✓	✓	
Software	✓			
Validation				
Formal analysis	✓	✓	✓	
Investigation	✓	✓	✓	✓
Resources				
Data curation	✓			
Writing – original draft	✓	✓	✓	✓
Writing – review and editing	✓	✓	✓	✓
Visualization	✓			
Supervision	✓	✓	✓	
Project administration				
Funding acquisition		✓		✓

Declaration of competing interest

The authors declare that they have no known competing financial interests or personal relationships that could have appeared to influence the work reported in this paper.

Acknowledgements

All the authors thank the two Referees for their suggestions, which helped to significantly improve this work. B.B. acknowledges the support

by the Italian Ministry of University and Research (MUR) through the PRIN 2020 project (No. 2020JLWP23) *Integrated Mathematical Approaches to Socio–Epidemiological Dynamics* (CUP: E15F21005420006). S.S.S. gratefully acknowledges the International Science Programme (ISP), Uppsala University, for their financial support for the research visit at Department of Mathematics and Applications of the University of Naples Federico II. He also gratefully acknowledges the Department of Mathematics and Applications of the University of Naples Federico II for kindly hosting him during September-December 2021. The present work has been performed under the auspices of the Italian National Group for the Mathematical Physics (GNFM) of National Institute for Advanced Mathematics (INdAM). The work has been also performed in the framework of 'NAASCO', bilateral agreement of scientific cooperation between the Department of Mathematics and Applications of the University of Naples Federico II and the Department of Mathematics of the Addis Ababa University.

References

[1] Bailey Norman TJ. The Mathematical Theory of Infectious Diseases and Its Applications. Second Edition. Charles Griffin & Company; 1975.
[2] Anderson Roy M, May Robert M. Infectious diseases of humans: dynamics and control. Oxford University Press; 1992.
[3] Keeling Matt J, Rohani Pejman. Modeling infectious diseases in humans and animals. Princeton University Press; 2011.
[4] Wang Zhen, Bauch Chris T, Bhattacharyya Samit, d'Onofrio Alberto, Manfredi Piero, Perc Matjaž, Perra Nicola, Salathé Marcel, Zhao Dawei. Statistical physics of vaccination. Physics Reports. 2016;664:1–113.
[5] Manfredi Piero, d'Onofrio Alberto. Modeling the interplay between human behavior and the spread of infectious diseases. New York: Springer; 2013.
[6] Capasso Vincenzo, Serio Gabriella. A generalization of the Kermack-Mckendrick deterministic epidemic model. Math Biosci. 1978;42(1–2):43–61.
[7] d'Onofrio Alberto, Manfredi Piero. Information–related changes in contact patterns may trigger oscillations in the endemic prevalence of infectious diseases. J Theor Biol. 2009;256(3):473–8.
[8] d'Onofrio Alberto, Manfredi Piero, Salinelli Ernesto. Vaccinating behaviour, information, and the dynamics of sir vaccine preventable diseases. Theor Popul Biol. 2007;71(3):301–17.
[9] Buonomo Bruno, Della Marca Rossella. Effects of information-induced behavioural changes during the covid-19 lockdowns: the case of Italy. R Soc Open Sci. 2020;7(10):201635.
[10] Aniţa Sebastian, Capasso Vincenzo, Arnăutu Viorel. An introduction to optimal control problems in life sciences and economics. New York: Birkhäuser/Springer; 2011.
[11] Kirk Donald E. Optimal control theory: an introduction. New Jersey: Prentice-Hall; 1970.
[12] Fleming Wendell H, Rishel Raymond W. Deterministic and stochastic optimal control, volume 1 of applications of mathematics. Berlin, New York: Springer; 1975.
[13] Schättler Heinz, Ledzewicz Urszula. Geometric optimal control: theory, methods and examples, volume 38 of interdisciplinary applied mathematics. New York: Springer; 2012.
[14] Morton Richard, Wickwire Kenneth H. On the optimal control of a deterministic epidemic. Adv Appl Probab. 1974;6(4):622–35.
[15] Miller Neilan Rachael L, Schaefer Elsa, Gaff Holly, Fister Renee K, Lenhart Suzanne. Modeling optimal intervention strategies for cholera. Bull Math Biol. 2010;72(8):2004–18.
[16] Onyango Nelson Owuor, Müller Johannes. Determination of optimal vaccination strategies using an orbital stability threshold from periodically driven systems. J Math Biol. 2014;68(3):763–84.
[17] Bolzoni Luca, Bonacini Elena, Della Marca Rossella, Groppi Maria. Optimal control of epidemic size and duration with limited resources. Math Biosci. 2019;315:108232.
[18] Arnăutu Viorel, Barbu Viorel, Capasso Vincenzo. Controlling the spread of a class of epidemics. Appl Math Optim. 1989;20(1):297–317.
[19] Lenhart Suzanne, Workman John T. Optimal control applied to biological models. London: CRC Press; 2007.
[20] Rodrigues Helena Sofia, Monteiro Teresa M, Torres Delfim FM. Vaccination models and optimal control strategies to dengue. Math Biosci. 2014;247:1–12.
[21] Sharomi Oluwaseun, Malik Tufail. Optimal control in epidemiology. Ann Oper Res. 2017;251(1–2):55–71.
[22] Biswas Santanu. Mathematical modeling of visceral leishmaniasis and control strategies. Chaos, Solitons Fractals. 2017;104:546–56.
[23] Lemos-Paião Ana P, Silva Cristiana J, Torres Delfim FM, Venturino Ezio. Optimal control of aquatic diseases: a case study of Yemen's cholera outbreak. J Optim Theory Appl. 2020:1–23.
[24] Bowong Samuel, Alaoui AMAziz. Optimal intervention strategies for tuberculosis. Commun Nonlinear Sci Numer Simul. 2013;18(6):1441–53.
[25] Betta Monica, Laurino Marco, Pugliese Andrea, Guzzetta Giorgio, Landi Alberto, Manfredi Piero. Perspectives on optimal control of varicella and herpes zoster by mass routine varicella vaccination. Proc R Soc Ser B. 2016;283(1826):20160054.
[26] Blayneh Kbenesh W, Gumel Abba B, Lenhart Suzanne, Clayton Tim. Backward bifurcation and optimal control in transmission dynamics of West Nile virus. Bull Math Biol. 2010;72(4):1006–28.
[27] Lee Sunmi, Golinski Michael, Chowell Gerardo. Modeling optimal age–specific vaccination strategies against pandemic influenza. Bull Math Biol. 2012;74(4):958–80.
[28] Barrett Scott, Hoel Michael. Optimal disease eradication. Environ Dev Econ. 2007;12(5):627–52.
[29] Nævdal Eric. Fighting transient epidemics—optimal vaccination schedules before and after an outbreak. Health Econ. 2012;21(12):1456–76.
[30] Rosa Silvério, Torres Delfim FM. Optimal control of a fractional order epidemic model with application to human respiratory syncytial virus infection. Chaos, Solitons Fractals. 2018;117:142–9.
[31] Bonyah Ebenezer, Gomez-Aguilar José Francisco, Adu Augustina. Stability analysis and optimal control of a fractional human african trypanosomiasis model. Chaos, Solitons Fractals. 2018;117:150–60.
[32] Kouidere Abdelfatah, Kada Driss, Balatif Omar, Rachik Mostafa, Naim Mouhcine. Optimal control approach of a mathematical modeling with multiple delays of the negative impact of delays in applying preventive precautions against the spread of the covid-19 pandemic with a case study of Brazil and cost-effectiveness. Chaos, Solitons Fractals. 2021;142:110438.
[33] Lü Xing, Hui Hong-wen, Liu Fei-fei, Bai Ya-li. Stability and optimal control strategies for a novel epidemic model of covid-19. Nonlinear Dyn. 2021:1–17.
[34] Abbasi Zohreh, Shafieirad Mohsen, Amiri Mehra Amir Hossein, Zamani Iman, Ibeas Asier. Optimal control design of impulsive sqeiar epidemic models with application to covid-19. Modeling, Control and Drug Development for COVID-19 Outbreak Prevention. Springer; 2022. p. 479–519.
[35] Buonomo Bruno, Della Marca Rossella, d'Onofrio Alberto. Optimal public health intervention in a behavioural vaccination model: the interplay between seasonality, behaviour and latency period. Math Med Biol J IMA. 2018:dqy011.
[36] Buonomo Bruno, Manfredi Piero, d'Onofrio Alberto. Optimal time-profiles of public health intervention to shape voluntary vaccination for childhood diseases. J Math Biol. 2019;78(4):1089–113.
[37] Della Marca Rossella, d'Onofrio Alberto. Volatile opinions and optimal control of vaccine awareness campaigns: chaotic behaviour of the forward-backward sweep algorithm vs. heuristic direct optimization. Commun Nonlinear Sci Numer Simul. 2021;98:105768.
[38] Misra AK, Sharma Anupama, Shukla JB. Stability analysis and optimal control of an epidemic model with awareness programs by media. Biosystems. 2015;138:53–62.
[39] Chen Yuyang, Bi Kaiming, Zhao Songnian, Ben-Arieh David, Wu Chih-Hang John. Modeling individual fear factor with optimal control in a disease-dynamic system. Chaos, Solitons Fractals. 2017;104:531–45.
[40] Ndii Meksianis Z, Adi Yudi Ari. Understanding the effects of individual awareness and vector controls on malaria transmission dynamics using multiple optimal control. Chaos, Solitons Fractals. 2021;153:111476.
[41] Das Parthasakha, Upadhyay Ranjit Kumar, Misra Arvind Kumar, Rihan Fathalla A, Das Pritha, Ghosh Dibakar. Mathematical model of covid-19 with comorbidity and controlling using non-pharmaceutical interventions and vaccination. Nonlinear Dyn. 2021:1–15.
[42] London Wayne P, Yorke James A. Recurrent outbreaks of measles, chickenpox and mumps: I. Seasonal variation in contact rates. Am J Epidemiol. 1973;98(6):453–68.
[43] Schwartz Ira B, Smith Hal L. Infinite subharmonic bifurcation in an seir epidemic model. J Math Biol. 1983;18(3):233–53.
[44] Aron Joan L, Schwartz Ira B. Seasonality and period-doubling bifurcations in an epidemic model. J Theor Biol. 1984;110(4):665–79.
[45] Earn David JD, Rohani Pejman, Bolker Benjamin M, Grenfell Bryan T. A simple model for complex dynamical transitions in epidemics. Science. 2000;287(5453):667–70.
[46] Buonomo Bruno, Chitnis Nakul, d'Onofrio Alberto. Seasonality in epidemic models: a literature review. Ricerche di Matematica. 2018;67(1):7–25.
[47] Goldstein Herbert, Poole Charles, Safko John. Classical mechanics. Pearson; 2014.
[48] Wiggins Stephen. Introduction to applied nonlinear dynamical systems and chaos. volume 2. Springer; 1990.
[49] Guckenheimer John, Holmes Philip. Nonlinear oscillations, dynamical systems, and bifurcations of vector fields. Springer; 1983.
[50] Holmes Catherine A, Holmes Philip J. Second order averaging and bifurcations to subharmonics in duffing's equation. J Sound Vib. 1981;78(2):161–74.
[51] Hale Jack K, Koçak Hüseyin. Dynamics and bifurcations. volume 3. Springer Science & Business Media; 2012.
[52] Vulpiani Angelo, Cecconi Fabio, Cencini Massimo. Chaos: from simple models to complex systems. World Scientific; 2009.
[53] Mandelstam Leonid I, Papalexi Nikolai D. Über resonanzerscheinungen bei frequenzteilung. Z Phys. 1932;73(3):223–48.
[54] Friedrichs Kurt O, Stoker James J. Forced vibrations of systems with nonlinear restoring force. Q Appl Math. 1943;1(2):97–115.
[55] Von Karman Théodore. The engineer grapples with nonlinear problems. Bull Am Math Soc. 1940;46(8):615–83.
[56] Minorsky Nicolai. Introduction to non-linear mechanics. Edwards; 1946.
[57] Smith Hal L. Subharmonic bifurcation in an sir epidemic model. J Math Biol. 1983;17(2):163–77.
[58] Smith Hal L. Multiple stable subharmonics for a periodic epidemic model. J Math Biol. 1983;17(2):179–90.
[59] Perkins Alex T, España Guido. Optimal control of the covid-19 pandemic with non-pharmaceutical interventions. Bull Math Biol. 2020;82(9):1–24.
[60] Vargas-De-León Cruz, d'Onofrio Alberto. Global stability of infectious disease models with contact rate as a function of prevalence index. Math Biosci Eng. 2017;14(4):1019.
[61] Efimov Denis V, Fradkov Alexander L. Yakubovich's oscillatority of circadian oscillations models. Math Biosci. 2008;216(2):187–91.
[62] Efimov Denis V, Fradkov Alexander L. Oscillatority of nonlinear systems with static feedback. SIAM J Control Optim. 2009;48(2):618–40.

[63] Smith Hal L. An introduction to delay differential equations with applications to the life sciences. volume 57. New York: Springer; 2011.
[64] Grass Dieter, Caulkins Jonathan P, Feichtinger Gustav, Tragler Gernot, Behrens Doris A, et al. Optimal control of nonlinear processes. Berlino: Springer; 2008.
[65] Pontryagin Lev S, Boltyanskii Vladimir G, Gamkrelidze Revaz V, Mishenko Evgenii F. The mathematical theory of optimal processes. (Translated from the Russian by Trigoroff, K. N.). New York: Wiley Interscience; 1962.
[66] Goenka Aditya, Liu Lin, Nguyen Manh-Hung. Infectious diseases and economic growth. J Math Econ. 2014;50:34–53.
[67] Bosi Stefano, Camacho Carmen, Desmarchelier David. Optimal lockdown in altruistic economies. J Math Econ. 2021;93:102488.
[68] Newbold Stephen C, Finnoff David, Thunström Linda, Ashworth Madison, Shogren Jason F. Effects of physical distancing to control covid-19 on public health, the economy, and the environment. Environ Resour Econ. 2020;76(4):705–29.
[69] d'Albis Hippolyte, Augeraud-Véron Emmanuelle. Optimal prevention and elimination of infectious diseases. J Math Econ. 2021;93:102487.
[70] Goenka Aditya, Liu Lin, Nguyen Manh-Hung. Sir economic epidemiological models with disease induced mortality. J Math Econ. 2021;93:102476.